Applied Physics Letters

RESEARCH ARTICLE | MARCH 09 2020

Effect of deposition temperature on ultra-low voltage resistive switching behavior of Fe-doped $SrTiO_3$ films

Xue Jiang (江雪); Minglong Wei (魏明龙); Cheuk Ho Chan; Yingyue Wang (王颖玥); Ruilian Lai (赖芮涟); Jianbo Wang (王建波); Jiyan Dai (戴吉岩); Xiaoyan Qiu (邱晓燕)

Appl. Phys. Lett. 116, 102101 (2020)
https://doi.org/10.1063/1.5123254

Applied Physics Letters ARTICLE scitation.org/journal/apl

Effect of deposition temperature on ultra-low voltage resistive switching behavior of Fe-doped $SrTiO_3$ films

Cite as: Appl. Phys. Lett. **116**, 102101 (2020); doi: 10.1063/1.5123254
Submitted: 5 August 2019 · Accepted: 24 February 2020 ·
Published Online: 9 March 2020

Xue Jiang (江雪),[1] Minglong Wei (魏明龙),[1] Cheuk Ho Chan,[2] Yingyue Wang (王颖玥),[1] Ruilian Lai (赖芮涟),[1] Jianbo Wang (王建波),[1] Jiyan Dai (戴吉岩),[2] and Xiaoyan Qiu (邱晓燕)[1,a)]

AFFILIATIONS

[1]School of Physical Science and Technology, Southwest University, Chongqing 400715, People's Republic of China
[2]Department of Applied Physics, The Hong Kong Polytechnic University, Hong Kong, People's Republic of China

[a)]Author to whom correspondence should be addressed: qxy2001@swu.edu.cn

ABSTRACT

The effect of deposition temperature on the microstructures and resistive switching properties of Fe-doped $SrTiO_3$ (Fe-STO) films deposited via magnetron sputtering has been investigated. The as-deposited Fe-STO films change from amorphous to polycrystalline when the deposition temperature increases to 600 °C, but 800 °C-deposited Fe-STO films exhibit cracked surface morphologies with Sr-rich nanosheet segregation. Fe-STO films deposited at ≤600 °C exhibit reversible bipolar resistive switching behaviors with ultra-low switching voltages of <±0.6 V, while 450 °C-deposited Fe-STO films retain an ON/OFF resistance ratio of ∼10^5 after more than 2500 endurance cycles and 600 °C-deposited Fe-STO films exhibit three different resistive switching patterns in sequence. Fe-assisted oxygen-vacancy conductive filaments are responsible for the ultra-low voltage resistive switching behaviors of Fe-STO films.

Under an external electric field, the resistances of some transition metal oxides (TMOs) can reversibly transition between two or more resistance states. This gives TMOs promising potential for applications in next-generation resistive switching random access memory (RRAM).[1] RRAM offers a simple metal-oxide-metal sandwich structure, low power consumption, and multi-level storage capacity. In addition, RRAM can emulate synapse behavior and therefore be used to implement neuromorphic computing and neural networks.[2–4] $SrTiO_3$ (STO) is a well-studied dielectric oxide whose electrical properties can vary systematically depending on its oxidation state and doping.[5] Thus, STO is an ideal system for investigating resistive switching phenomena. However, stoichiometric STO films are highly insulating and typically require an electroforming process to enable resistive switching behavior. Typical STO-based RRAM switching voltages exceed 1 V,[6–14] but Yan *et al.*[15] have reported reproducible Ag/STO/Pt memory cell resistive switching behavior at voltages lower than 0.5 V. They attribute this low-voltage resistive behavior to Ag^+ ion conductive filaments (CFs). Dopant metal ions,[16–32] such as Bi, Nb, Cr, Nd, La, and Fe, organic molecules,[33] thermal treatment,[34,35] and ultraviolet irradiation[36] can introduce various point defects into STO films. These defects can significantly improve ON/OFF ratios, but have little effect on the endurance and retention properties. Inserting metal/oxide buffer layers such as Ti,[37] Ta,[38] and NiO[39] between the STO film and electrodes can improve endurance and retention properties, but typically increases the switching voltage.

In this paper, Fe-STO films with an Fe concentration of 3 at. % were deposited on Pt-covered Si(100) wafers at various deposition temperatures (T_d) via magnetron sputtering. Ag/Fe-STO/Pt memory cells made using 450 °C-deposited amorphous Fe-STO films exhibit excellent bipolar resistive switching characteristics. A device with an ON/OFF ratio of ∼10^5 can exceed 2500 cycles with a switching voltage of less than ±0.6 V. This is substantially better than that has been reported for Fe-STO films in previous literature studies[27–32] and indicates potential amorphous Fe-STO film applications in low-operating voltage RRAM and artificial neuron synapses. Moreover, 600 °C-deposited polycrystalline Fe-STO films exhibit unique cycling-dependent resistive switching patterns. These give us a new way to understand resistive switching degradation mechanisms. In contrast to the report by Yan *et al.*,[15] our micro-structural investigation results reveal that this low voltage, high ratio resistive switching behavior is driven by Fe-assisted oxygen vacancy ($V_o^{\cdot\cdot}$) CFs rather than Ag^+ ion CFs.

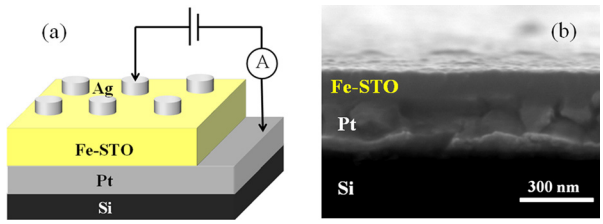

FIG. 1. (a) Schematic diagram of the Ag/Fe-STO/Pt memory cell and (b) cross-sectional SEM image of an Fe-STO film deposited on a Pt-covered Si substrate.

Fabrication details and characterization studies of the Ag/Fe-STO/Pt memory cell illustrated in Fig. 1(a) are presented in the supplementary material. Figure 1(b) shows a cross-sectional SEM image of an Fe-STO film deposited on a Pt-covered Si substrate. The Fe-STO film is ~80 nm thick and exhibits a clear Fe-STO/Pt interface. Figures 2(a)–2(d) show the top-view SEM images of Fe-STO films deposited at different T_d values. The films deposited at 250 °C and 450 °C exhibit similar dense, smooth surface morphologies, while the film deposited at 600 °C exhibits a nano-scale cracked surface with an average grain diameter of ~50 nm [Figs. 2(a)–2(c)]. When the T_d increases to 800 °C because of thermal stress during the deposition and annealing process, the 800 °C-deposited Fe-STO film is fragmented with some nano-sheets segregated on the surface [Fig. 2(d)]. This implies possible Fe-STO film phase separation at 800 °C. We subsequently investigated the elemental composition and distribution of the 800 °C-deposited Fe-STO film via EDS and selected area studies. Sr, Ti, and Fe elemental maps [Figs. 2(e)–2(g)] exhibit similar uniform distributions, but the energy dispersive spectrometer (EDS) spectra of the selected areas with and without nano-sheets (areas A and B) are quite different. The normalized Sr at. % is significantly higher in area A than in area B while the situation for Ti is inverted [Fig. 2(h)]. This implies that nano-sheets segregated on the 800 °C-deposited Fe-STO film surface are Sr-rich. Similar Sr segregation phenomena have been observed on STO film surfaces during electroforming.[31] There is no obvious difference between the normalized Fe at. % data in areas A and B, which indicates uniform Fe atom distributions in STO films, even at 800 °C.

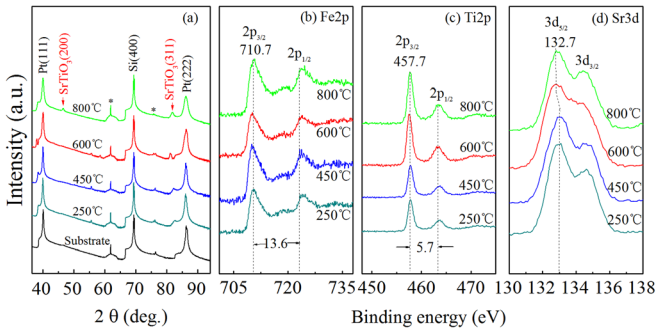

FIG. 3. (a) XRD and XPS spectra of (b) Fe2p, (c) Ti2p, and (d) Sr3d core levels for Fe-STO films deposited at 250 °C, 450 °C, 600 °C, and 800 °C, respectively.

The crystal structures and chemical compositions of Fe-STO films deposited at various T_d values were investigated via XRD and XPS, respectively. As shown in Fig. 3(a), only Pt(111), Pt(222), and Si (400) plane peaks and diffraction peaks from impurities (marked with asterisks) in the Pt-covered Si substrate are observed in the 250 °C and 450 °C-deposited Fe-STO films. No other diffraction peaks are noted from STO. The diffraction peak from the STO(311) plane (PDF #35–0734) is first observed in the 600 °C-deposited Fe-STO film, while that corresponding to the STO(200) plane is first observed in the 800 °C-deposited Fe-STO film. XRD analyses reveal that Fe-STO films deposited at ≥600 °C are polycrystalline. No Fe signal is observed in any XRD spectrum. This may be because very few Fe atoms are doped into the STO film (~3 at. %).

Fe-STO films deposited at different T_d values were analyzed via XPS to identify the chemical valences of the doped-Fe atoms. As shown in Fig. 3(b), the $Fe2p_{3/2}$ core level is fixed at 710.7 eV and does not shift when T_d increases. This indicates that the Fe atoms doped onto the STO film surface are Fe^{3+} ions.[40] $Ti2p_{3/2}$ core levels remain at 457.7 eV without any shift as T_d increases [Fig. 3(c)]. This binding energy is consistent with Ti^{4+} ions in perovskite STO films.[41,42] However, the $Sr3d_{5/2}$ core level exhibits a slight red shift from 132.9 eV to 132.7 eV when the T_d increases from 450 °C to 600 °C, as shown in

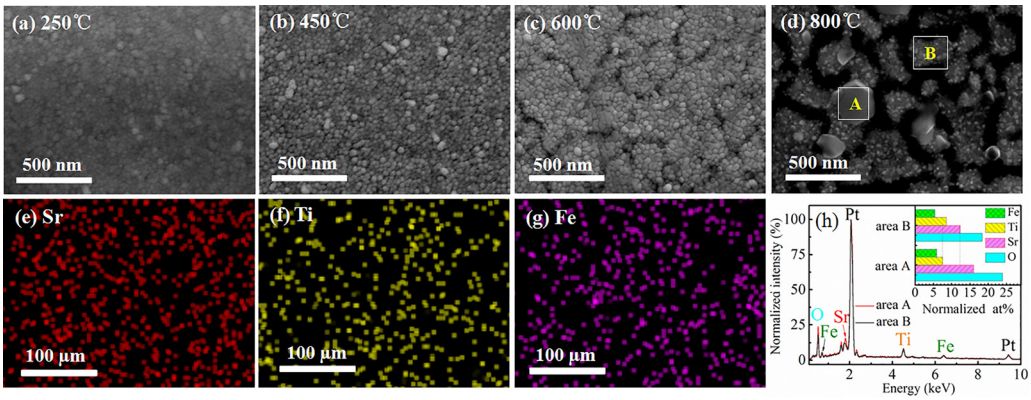

FIG. 2. Top-view SEM images of Fe-STO films deposited at (a) 250 °C, (b) 450 °C, (c) 600 °C, and (d) 800 °C, respectively. (e) Sr, (f) Ti, and (g) Fe EDS maps of the 800 °C-deposited Fe-STO film. (h) EDS spectra of areas A and B [marked with squares in (d)]. The inset in (h) shows Fe, Sr, Ti, and O at. % data normalized by using the strongest Pt peak as the reference.

Fig. 3(d). This further confirms surface segregation of Sr in Fe-STO films deposited at $T_d \geq 600\,^{\circ}C$. Therefore, we subsequently measured the XPS depth profiles of 450 °C- and 600 °C-deposited Fe-STO films. As shown in Figs. S1(a), S1(b), S2(a), and S2(b) in the supplementary material, no Ag ions diffuse into either the Fe-STO film and Ti2p core levels do not change with the etch depth. However, the $Sr3d_{5/2}$ core level in the 600 °C-deposited Fe-STO film shifts slightly from 132.7 eV to 132.9 eV when the film is etched to a depth of ~40 nm [Fig. S2(c), supplementary material]. This implies that the Sr shift depth is about 40 nm. Similar Sr shift phenomena have also been observed in Fe-STO films deposited at 700 °C via pulsed laser deposition.[43] On the other hand, both the 450 °C- and 600 °C-deposited Fe-STO films are heavily oxygen deficient since the Fe^0 and Fe^{2+} peaks at 706.3 eV and 708.7 eV, respectively[40] are observed in their Fe2p core-level XPS depth profiles [Figs. S1(d) and S2(d), supplementary material].

After applying a gate voltage (V_g) to the Ag top electrode, Ag/Fe-STO/Pt memory cell current–voltage (I–V) curves were characterized by sweeping the V_g in a $0 \rightarrow +V_g \rightarrow 0 \rightarrow -V_g \rightarrow 0$ sequence (denoted by numbered arrows). All of the Fe-STO films deposited at various T_d values exhibit stable, reversible bipolar resistive switching behaviors with set/reset voltages (V_{Set}/V_{Reset}) lower than ±0.6 V. As shown in Figs. 4(a) and 4(b), 250 °C and 450 °C-deposited Fe-STO films exhibit similar I–V loops with a steep set/reset process. At a reading voltage (V_r) of 0.2 V, the 250 °C-deposited film achieves an ON/OFF ratio of 10^4–10^5 for ~390 cycles, while the 450 °C-deposited film achieves a higher ON/OFF ratio of 10^5 for more than 2500 cycles. The 600 °C-deposited polycrystalline Fe-STO film exhibits three different "set" patterns in sequence in the positive voltage region. As shown in Fig. 4(c), this starts with a "one step set pattern" (Pattern P1) with an initial ON/OFF ratio of $>10^4$ at $V_r = 0.1$ V. After ~1100 cycles, Pattern P1 changes to the "two step set pattern" (Pattern P2) for a further 1000 cycles. Finally, Pattern P2 degrades to another "one step set pattern" (Pattern P3) with a lower ON/OFF ratio of $\sim 10^2$ for ~700 cycles until the memory cell ceases to exhibit resistive switching behavior. We think that these cycling-dependent resistive switching patterns can be attributed to decreased oxygen vacancy concentrations caused by further oxidization of doped Fe atoms during the I–V measurement. XPS depth profiles of Fe2p core levels (Fig. S3, supplementary material) for the 600 °C-deposited Fe-STO film before and after 2800 I–V cycles clearly demonstrate this. A detailed discussion is given in the supplementary material. The I–V loops of the 800 °C-deposited Fe-STO film exhibit an ON/OFF ratio of <5 at $V_r = 0.2$ V and a poor endurance of ~50 cycles [Fig. 4(d)]. Upon combining this information with the SEM images and the EDS spectra shown in Fig. 2, we determined that the cracked film and Sr-rich nano-sheet surface segregation decrease the resistance of the 800 °C-deposited Fe-STO film, resulting in a disastrous degradation of the resistive switching properties. Thus, we subsequently discuss only the resistive switching characteristics of Fe-STO films deposited at $T_d \leq 600\,^{\circ}C$.

To characterize Ag/Fe-STO/Pt memory cell stability, we investigated the variation in the high/low resistive state (R_H/R_L) resistances with cycle numbers, and V_{Set}/V_{Reset} distributions using Fe-STO films deposited at $T_d \leq 600\,^{\circ}C$. As shown in Figs. 5(a) and 5(b), the 250 °C-deposited film can retain an ON/OFF ratio of 10^4–10^5 after ~390 endurance cycles, while the 450 °C-deposited film retains a higher ON/OFF ratio of 10^5 after more than 2500 endurance cycles, which indicates better cycling endurance properties. For the 600 °C-deposited polycrystalline film, the P1 and P2 patterns maintain an ON/OFF ratio of 10^4–10^5 for more than 2100 cycles, while the P3 pattern continues for only ~700 cycles and has a lower ON/OFF ratio of $\sim 10^2$ before the memory cell fails to perform resistive switching [Fig. 5(c)]. Figures 5(d)–5(f) show V_{Set}/V_{Reset} cumulative probability distributions for Fe-STO films deposited at $T_d \leq 600\,^{\circ}C$. The amplitudes of V_{Set} and V_{Reset} gradually decrease as T_d increases. We think that the Fe-STO film crystallinity improvement that occurs when T_d increases is responsible for the decrease in V_{Set}/V_{Reset}.

In order to characterize memory cell reliability, we also investigated the ON/OFF ratio, V_{Set}, and V_{Reset} error distributions using five different cells (C1–C5) made from Fe-STO films deposited at different T_d values. The data were extracted from 100 I–V cycles per memory cell. Figure 6 compares the Fe-STO films deposited at 250 °C–600 °C. Those deposited at 450 °C exhibit higher ON/OFF ratios and narrower V_{Set}/V_{Reset} fluctuations, indicating better reliability. One possible reason for this is that the 450 °C-deposited film is denser than the

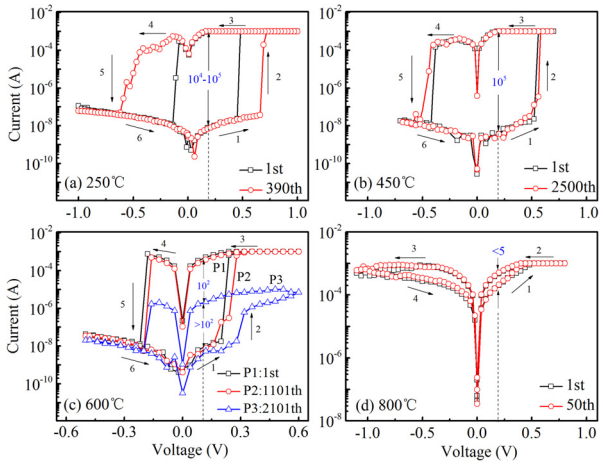

FIG. 4. Consecutive I–V curves for Fe-STO films deposited at (a) 250 °C, (b) 450 °C, (c) 600 °C, and (d) 800 °C, respectively.

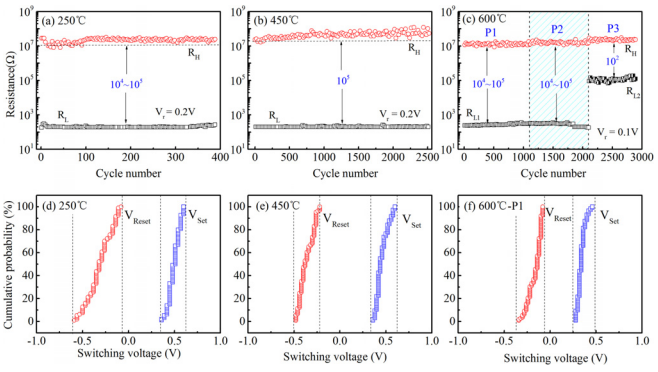

FIG. 5. (a)–(c) Variation in R_H/R_L with cycle number and (d)–(f) V_{Set}/V_{Reset} cumulative probability distributions for Fe-STO films deposited at 250 °C, 450 °C, and 600 °C, respectively.

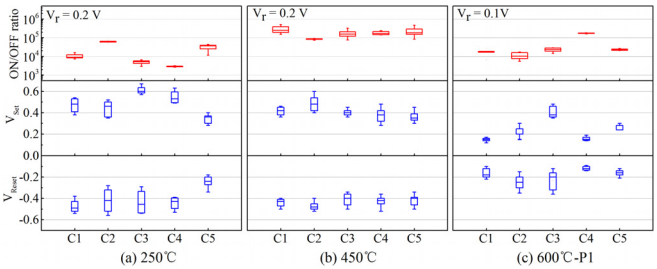

FIG. 6. ON/OFF ratio, V_{Set}, and V_{Reset} error distributions for five different memory cells (C1–C5) with Fe-STO films deposited at (a) 250 °C, (b) 450 °C, and (c) 600 °C, respectively.

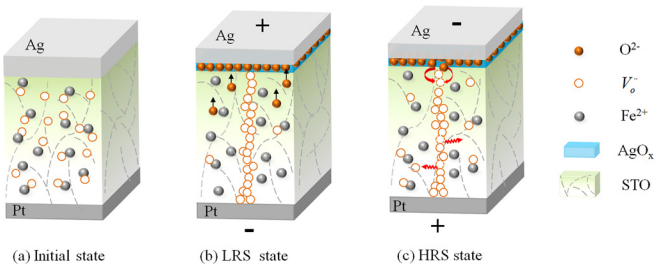

FIG. 7. Schematic diagrams of O^{2-} ion and $V_o^{\cdot\cdot}$ vacancy distributions in Ag/Fe-STO/Pt memory cells in their (a) initial, (b) LRS, and (c) HRS states.

250 °C-deposited film but more homogenous than the 600 °C-deposited film.

Table I shows the key resistive switching performance results for Fe-STO films deposited at various T_d values. The 450 °C -deposited Fe-STO films exhibit the best resistive switching properties: a high ON/OFF ratio of 10^5 at a V_r of 0.2 V, a good endurance of ~2500 cycles, and V_{Set}/V_{Reset} voltages lower than ±0.6 V. Compared to devices from previous reports on various STO-based memory cells[6–32] that are summarized in Table SI in the supplementary material, our device offers a higher ON/OFF ratio but lower V_{Set}/V_{Reset} voltages, which indicates potential for ultra-low operating voltage resistive switching device applications.

The metal ion-CF mechanism[13–15] is commonly referenced to explain STO-based memory cells with active metal electrodes such as Ag, Cu, and Al. Interfacial mechanisms[16–22] attribute the resistive switching behavior to Schottky-barrier changes (SBCs) or space-charge limited current (SCLC) induced by an applied electric field. In contrast, vacancy or defect-CF mechanisms[23–31] attribute it to CFs composed of various point defects, such as Sr (V''_{Sr}) or oxygen ($V_o^{\cdot\cdot}$) vacancies, Sr antisite defects with associated oxygen vacancies ($Sr''_{Ti} - V_o^{\cdot\cdot}$), and screw dislocations. Both CF and interface-type mechanisms can coexist.[6,7,32] Experimental results and theoretical calculations[27] have shown that $V_o^{\cdot\cdot}$ vacancies are the dominant defect in Fe-doped STO, and that they prefer to cluster in the first coordination shell around Fe atoms.[28] The Fe-STO films in our work contain no Ag ions, but substantial oxygen-deficiencies are present. Thus, we hypothesize the presence of concentrated $V_o^{\cdot\cdot}$ vacancies around Fe atoms in initial Fe-STO films, as shown in Fig. 7(a). When a positive bias is applied to the Ag top electrode, oxygen ions drift from the Fe-STO film to the Ag electrode and react with Ag to form AgO_x. Simultaneously, new $V_o^{\cdot\cdot}$ vacancies emerge in the Fe-STO film. These new $V_o^{\cdot\cdot}$ vacancies combine with the preexisting $V_o^{\cdot\cdot}$ vacancies around Fe atoms to form CFs that bridge the top and bottom electrodes. As a result, the memory cell transitions to a low resistance state (LRS), as shown in Fig. 7(b). In contrast, applying a negative bias to the Ag electrode causes oxygen ions to drift back into the film, where they recombine with $V_o^{\cdot\cdot}$ vacancies near the Ag electrode. This results in CF rupture near the Ag electrode and the memory cell transitions to a high resistance state (HRS) [Fig. 7(c)]. Due to the large LRS leakage current, the joule heat effect accelerates the rupture of $V_o^{\cdot\cdot}$ vacancy CFs, consequently decreasing the V_{Reset} voltage. On the other hand, increasing the T_d produces as-deposited Fe-STO films that are polycrystalline (≥600 °C) instead of amorphous. Increased grain boundary defects enhance $V_o^{\cdot\cdot}$ vacancy CF formation and thus the V_{Set} voltage decreases as T_d increases.

In summary, we investigated the microstructures and resistive switching behaviors of Fe-STO films deposited at various temperatures. Films deposited at 250 °C and 450 °C were amorphous Fe-STO films with smooth, dense surfaces, while 600 °C-deposited Fe-STO films were polycrystalline with an average grain size of 50 nm and 800 °C-deposited Fe-STO films exhibited cracked morphologies and surface segregation of Sr-rich nano-sheets. Amorphous, 450 °C-deposited Fe-STO films exhibited the best bipolar resistive switching characteristics: an ultra-low switching voltage of <±0.6 V, a high ON/OFF ratio of ~10^5, and a good endurance of more than 2500 cycles. Polycrystalline Fe-STO films deposited at 600 °C exhibited cycling-dependent resistive switching patterns. Doped Fe atoms enhanced oxygen vacancy CF formation in STO films, thus significantly decreasing switching voltages. This indicates potential applications in low-voltage resistive switching memory devices.

TABLE I. Resistive switching properties of Fe-STO films deposited at various T_d values.

T_d (°C)	V_{Set} (V)	V_{Reset} (V)	ON/OFF ratio at V_r	Endurance (cycle)
250	0.28–0.67	−0.18 to −0.56	10^4–10^5 at 0.2 V	390
450	0.28–0.6	−0.34 to −0.52	10^5 at 0.2 V	2500
600	P1: 0.12–0.48	−0.09 to −0.36	10^4–10^5 at 0.1 V	1100
	P2: 0.16–0.46	−0.1 to −0.34	10^4–10^5 at 0.1 V	1000
	P3: 0.2–0.3	−0.1 to −0.34	10^2 at 0.1 V	700
800	>0.4	~−1	<5 at 0.2 V	~50

See the supplementary material for the details of film deposition, memory cell fabrication, micro-structural characterization, and I–V measurement. A discussion of the XPS depth profiles of the 450 °C- and 600 °C-deposited Fe-STO films before and after the I–V cycle measurement is also provided. Comparisons of resistive switching characteristics and mechanisms for various STO-based memory cells are presented in Table SI.

This work was supported by the National Natural Science Foundation of China (Grant No. 11274257), the Natural Science Foundation of Chongqing (Grant No. cstc2019jcyj-msxmX0451), and the Fundamental Research Fund for the Central Universities (Grant No. XDJK2018B034). The authors would also like to thank Dr. Kai Zhou at the Analytical and Testing Center of Chongqing University for the assistance with XPS depth profile measurements.

REFERENCES

[1]R. Waser, R. Dittmann, G. Staikov, and K. Szot, Adv. Mater. **21**, 2632 (2009).
[2]X. L. Hong, D. J. J. Loy, P. A. Dananjaya, F. Tan, C. M. Ng, and W. S. Lew, J. Mater. Sci. **53**(12), 8720 (2018).
[3]Q. F. Xia and J. J. Yang, Nat. Mater. **18**(4), 309 (2019).
[4]H. S. Jeong and L. P. Shi, J. Phys. D **52**, 023003 (2019).
[5]T. Tomio, H. Miki, H. Tabata, T. Kawai, and S. Kawai, J. Appl. Phys. **76**(10), 5886 (1994).
[6]X. Guo, Appl. Phys. Lett. **101**(15), 152903 (2012).
[7]M. Kubicek, R. Schmitt, F. Messerschmitt, and J. L. M. Rupp, ACS Nano **9**(11), 10737 (2015).
[8]C. Baeumer, C. Schmitz, A. H. H. Ramadan, H. Du, K. Skaja, V. Feyer, P. Müller, B. Arndt, C. L. Jia, J. Mayer, R. A. De Souza, C. M. Schneider, R. Waser, and R. Dittmann, Nat. Commun. **6**, 8610 (2015).
[9]A. Thakre and A. Kumar, Vacuum **151**, 182 (2018).
[10]X. B. Yan, Y. D. Xia, H. N. Xu, X. Gao, H. T. Li, R. Li, J. Yin, and Z. G. Liu, Appl. Phys. Lett. **97**(11), 112101 (2010).
[11]D. Y. Zhang, H. Hong, and Z. Luo, in Proceedings of IEEE International Nanoelectronics Conference (2016), p. 1.
[12]X. X. Liao, Y. F. Zhang, J. O. Wang, J. Y. Kang, J. B. Zhang, J. Z. Wang, J. C. Zheng, and H. Q. Wang, Materials **12**, 3698 (2019).
[13]T. Wan, B. Qu, H. W. Du, X. Lin, Q. R. Lin, D.-W. Wang, C. Cazorla, S. Li, S. D. Liu, and D. W. Chu, J. Colloid Interface Sci. **512**, 767 (2018).
[14]P. F. Hou, Z. Z. Gao, and K. K. Ni, RSC Adv. **7**, 49753 (2017).
[15]X. B. Yan, K. Li, J. Yin, Y. D. Xia, H. X. Guo, L. Chen, and Z. G. Liu, Electrochem. Solid-State Lett. **13**(3), H87 (2010).
[16]H. Wang, W. B. Zhang, J. W. Xu, G. B. Liu, H. Xie, and L. Yang, Bull. Mater. Sci. **41**, 149 (2018).
[17]S. K. Wang, X. W. Sun, G. H. Li, C. H. Jia, G. Q. Li, and W. F. Zhang, Nanoscale Res. Lett. **13**, 18 (2018).
[18]D. L. Xu, Y. Xiong, M. H. Tang, B. W. Zeng, Y. G. Xiao, and Z. P. Wang, Chin. Phys. B **22**(11), 117314 (2013).
[19]X. G. Chen, X. B. Ma, Y. B. Yang, L. P. Chen, G. C. Xiong, G. J. Lian, Y. C. Yang, and J. B. Yang, Appl. Phys. Lett. **98**, 122102 (2011).
[20]Y. D. Zhu, M. Y. Li, H. Zhou, Z. Q. Hu, X. L. Liu, X. L. Fang, B. Sebo, G. J. Fang, and X. Z. Zhao, J. Phys. D **45**, 375303 (2012).
[21]S. Q. Ren, G. C. Zhu, J. H. Xie, J. P. Bu, H. W. Qin, and J. F. Hu, J. Phys.: Condens. Matter **28**, 056001 (2016).
[22]M. Y. Song, Y. Seo, Y. S. Kim, H. D. Kim, H.-M. An, B. H. Park, Y. M. Sung, and T. G. Kim, Appl. Phys. Express **5**, 091202 (2012).
[23]T. Wan, B. Qu, H. W. Du, X. Lin, P. Y. Guan, Q. R. Lin, N. Chen, T. T. Tan, T. Hang, and D. Chu, J. Colloid Interface Sci. **494**, 178 (2017).
[24]X. B. Yin, Z. H. Tan, R. Yang, and X. Guo, J. Electroceram. **39**, 210 (2017).
[25]J. Park, D. H. Kwon, H. Park, C. U. Jung, and M. Kim, Appl. Phys. Lett. **105** (18), 183103 (2014).
[26]J. C. Li, G. Yang, Y. H. Wu, W. F. Zhang, and C. H. Jia, Phys. Status Solidi A **215**, 1700912 (2018).
[27]M. Kubicek, S. Taibl, E. Navickas, H. Hutter, G. Fafilek, and J. Fleig, J. Electroceram. **39**, 197 (2017).
[28]C. Lenser, A. Kuzmin, J. Purans, A. Kalinko, R. Waser, and R. Dittmann, J. Appl. Phys. **111**(7), 076101 (2012).
[29]T. Menke, P. Meuffels, R. Dittmann, K. Szot, and R. Waser, J. Appl. Phys. **105** (6), 066104 (2009).
[30]Ch. Lenser, Z. Connell, A. Kovács, R. Dunin-Borkowski, A. Köhl, R. Waser, and R. Dittmann, Appl. Phys. Lett. **102**(18), 183504 (2013).
[31]Ch. Lenser, A. Koehl, L. Slipukhina, H. C. Du, M. Patt, V. Feyer, C. M. Schneider, M. Lezaic, R. Waser, and R. Dittmann, Adv. Funct. Mater. **25**(40), 6360 (2015).
[32]R. Muenstermann, T. Menke, R. Dittmann, and R. Waser, Adv. Mater. **22**(43), 4819 (2010).
[33]G. L. Chen, P. Zhang, L. L. Pan, L. Qi, F. C. Yu, and C. X. Gao, J. Mater. Chem. C **5**(2), 9799 (2017).
[34]K. Szot, W. Speier, R. Carius, U. Zastrow, and W. Beyer, Phys. Rev. Lett. **88**(7), 075508 (2002).
[35]X. Q. Pan, Y. Shuai, C. G. Wu, W. B. Luo, X. Y. Sun, Y. Yuan, S. Q. Zhou, X. Ou, and W. L. Zhang, Appl. Surf. Sci. **389**, 1104 (2016).
[36]S. Suwanwong, T. Eknapakul, Y. Rattanachai, C. Masingboon, S. Rattanasuporn, R. Phatthanakun, H. Nakajima, P. D. C. King, S. K. Hodak, and W. Meevasana, Appl. Surf. Sci. **355**, 210 (2015).
[37]H. Nili, S. Walia, S. Balendhran, D. B. Strukov, M. Bhaskaran, and S. Sriram, Adv. Funct. Mater. **24**(43), 6741 (2014).
[38]A. Tsurumaki-Fukuchi, R. Nakagawa, M. Arita, and Y. Takahashi, ACS Appl. Mater. Interfaces **10**, 5609 (2018).
[39]X. W. Sun, C. H. Jia, X. S. Liu, G. Q. Li, and W. F. Zhang, Chin. Phys. B **27**(4), 047304 (2018).
[40]T. Yamashita and P. Hayes, Appl. Surf. Sci. **254**(8), 2441 (2008).
[41]S. Fuentes, P. Muñoz, N. Barraza, E. Chávez-Ángel, and C. M. Sotomayor Torres, J. Sol-Gel Sci. Technol. **75**(3), 593 (2015).
[42]O. Lobacheva, Y. M. Yiu, N. Chen, T. K. Sham, and L. V. Goncharova, Appl. Surf. Sci. **393**, 74 (2017).
[43]J. Szadea, K. Szot, M. Kulpa, J. Kubacki, Ch. Lenser, R. Dittmann, and R. Waser, Phase Transitions **84**(5-6), 489 (2011).